Running head: Environmental synchrony and dispersal in Taylor's law

Title: **Effects of environmental synchrony and density-dependent dispersal on temporal and spatial slopes of Taylor's law**

Author: Takashi Saitoh

Field Science Center, Hokkaido University, North-11, West-10, Sapporo 060-0811, Japan

Email: tsaitoh@fsc.hokudai.ac.jp

ORCiD ID: 0000-0003-4085-5014

Abstract

Taylor's law (TL) is an empirical rule that describes an approximate relationship between the variance and mean of population density: $\log_{10}(\text{variance}) \approx \log_{10}(a) + b \times \log_{10}(\text{mean})$. Population synchrony is another prevailing feature observed in empirical populations. This study investigated the effects of environmental synchrony and density-dependent dispersal on the temporal (b_T) and spatial (b_S) slopes of TL, using an empirical dataset of grey-sided vole populations and simulation analyses based on the second-order autoregressive (AR) model. Eighty-five empirical populations satisfied the temporal and spatial TLs with $b_T = 1.943$ (± SE 0.143) and $b_S = 1.579$ (± SE 0.136). The pairwise synchrony of population was 0.377 ± 0.199 (mean ± SD). Most simulated populations that obeyed the AR model satisfied the form of the temporal and spatial TLs without being affected by the environmental synchrony and density-dependent dispersal; however, those simulated slopes were too steep. The incorporation of environmental synchrony resulted in reduced simulated slopes, but those slopes, too, were still unrealistically steep. By incorporating density-dependent dispersal, simulated slopes decreased and fell within a realistic range. However, the simulated populations without environmental synchrony did not exhibit an adequate degree of density synchrony. In simulations that included both environmental synchrony and density-dependent dispersal, 92.7% of the simulated datasets provided realistic values for b_T, b_S, and population synchrony. Because the two slopes were more sensitive to the variation of density-dependent dispersal than that of environmental synchrony, density-dependent dispersal may be the key to the determination of b_T and b_S.

KEY WORDS:

autoregressive time series, density dependence, environmental variability, rodents, slope, Taylor's law

1 | INTRODUCTION

Taylor's law (TL, Taylor 1961) is an empirical rule describing the approximate relationship between the variance and mean of population densities, in which the variance is given by a power-law function of the mean: variance $\approx a \times (\text{mean})^b$, $a > 0$. It is usually expressed as:

$$\log_{10}(\text{variance}) \approx \log_{10}(a) + b \times \log_{10}(\text{mean}). \quad \text{(Eq. 1)}$$

The mean and variance of population densities can be calculated based on variations through both time and space. In the temporal TL, the mean and variance are calculated through observations of population densities at different times in a given location, while in the spatial TL, they are calculated through observations of population densities at different locations over a given time.

The temporal and spatial TLs are described by the same equation given above (Eq. 1), and both TLs have been widely verified in various ecological systems (Taylor, 1986) and other research fields (Eisler, Bartos, & Kertész, 2008; Tippett & Cohen, 2016). Another well-known feature of TLs is the range of slopes; most of the observed slopes (b) fall between 1 and 2 for both TLs (Downing, 1986; Kendal, 2004; Taylor, 1961). However, the underlying mechanism of the temporal and spatial TLs still remains unclear, and a very few studies have considered both of these TLs (Taylor & Woiwod, 1982; Zhao, Sheppard, & Reid, 2019). Are the temporal and spatial TLs govern by the same factors? By examining the similarities and dissimilarities in the features of the temporal and spatial TLs, a deeper insight into the mechanism of the TL formation can be gained.

A model simulation is an approach for checking the plausibility of a chosen mechanistic explanation in a complex system. Saitoh and Cohen (2018) showed that sustainable populations could obey the temporal TL even in the absence of synchrony and density-dependent movement among populations and identified the conditions that produced slopes $1 < b_T < 2$ by intensive simulation analyses for population densities of the grey-sided

vole, *Myodes rufocanus* (Sundevall, 1846), in Hokkaido (see also Cohen & Saitoh, 2016). However, dispersal has been recognized as being capable of producing both spatial stability and synchrony of population density (Abbott 2011), and density-dependent movement of individuals among populations may affect the slope of TL (Perry, 1988; Taylor & Taylor, 1977). In addition, most field populations are typically subjected to correlated environmental influences (i.e., the Moran effect: Moran, 1953) (Allstadt et al., 2015). Although Saitoh and Cohen (2018) demonstrated that synchrony and density-dependent movement among populations are not sufficient conditions for the temporal TL, those effects were not examined for the spatial TL. Field populations inhabit areas with varying quality, and density-dependent movement from a higher- to a lower-density population could reduce the mean of population densities in higher-quality habitats while enhancing the mean in lower-quality habitats. Consequently, density-dependent movements could lower the variance of population densities and reduce the slope of TL, as Taylor and Taylor (1977) and Perry (1988) suggested. Population synchrony could also reduce the slopes of TL (Reuman et al., 2017). The temporal and spatial TLs may be related to each other, and environmental synchrony and density-dependent movement may influence these TLs by synchronizing population dynamics or leveling population densities. Therefore, to gain a more comprehensive understanding of the two TLs and a deeper insight into the formation of TL, it would be useful to analyze the relationship between these three population features (the temporal TL, and the spatial TL, and the population synchrony), and environmental synchrony and density-dependent movement should be taken into consideration because they may help establish this relationship.

This study reports on the temporal and spatial TLs for the empirical populations of the grey-sided vole and on simulation analyses to explore determinants of TL slopes using the Gompertz model with extensive combinations of model parameters. First, this study reveals

that most sustainable populations conform to both the temporal and spatial TLs in the absence of population synchrony and density-dependent movement among populations. Next, it identifies the combinations of model parameters that are likely to produce the prevailing slopes $1 < b < 2$ for the temporal and spatial TLs and shows how the observed coefficients of the Gompertz model satisfy those identified combinations for the temporal TL, but not for the spatial TL. To solve this discrepancy, the effects of environmental synchrony and density-dependent movement are incorporated into a simulation model. Finally, the relative contribution of environmental synchrony and density-dependent movement in generating the observed features of the temporal and spatial TLs and population synchrony is discussed.

2 | MATERIALS AND METHODS

2.1 | Study design and data

Hokkaido is the northernmost island of Japan (78,073 km^2). The grey-sided vole, *Myodes rufocanus* (Sundevall, 1846), is the most common species of small rodents on this island (Kaneko et al., 1998). A systematic survey of rodent populations has been carried out in Hokkaido by the Forestry Agency of the Japanese Government. The geography of Hokkaido and the procedure of data collection were described previously (Saitoh, Stenseth, & Bjørnstad, 1997, 1998; Stenseth et al., 2003). This study analyzed the same dataset of the grey-sided vole as Cohen and Saitoh (2016) and Saitoh and Cohen (2018) did: $N = 85$ populations in different locations covering $T = 31$ years (1962–1992). Population density was defined as the number of voles per 150 trap-nights, because 50 snap-traps for three consecutive nights on a 0.5 ha survey plot was chosen as a standard unit for the rodent survey.

The Bayesian method was applied to the estimation of population density for each year and location based on a state-space model on WinBUGS version 1.4.3 (Spiegelhalter et

al., 2003; http://www.mrc-bsu.cam.ac.uk/software/bugs/). Population density was estimated assuming that the increase in the number of voles caught was proportional to the trapping effort, taking effective traps into consideration (see Saitoh & Cohen, 2018 for details). Although the natural logarithm of the number of individual voles trapped per unit of trapping effort (one trap-night) was used, the estimates were reverted to the original scale of measurement, the vole density per 150 trap-nights, for the following analyses of TL.

2.2 | Temporal and spatial Taylor's laws

The mean and the variance were calculated across the density estimates in a given location at different times (years in this study), and one data point [$\log_{10}$(temporal mean), $\log_{10}$(temporal variance)] was plotted for each location (n = 85). The mean and variance were calculated across the density estimates in a given year at different locations, and one data point [$\log_{10}$(spatial mean), $\log_{10}$(spatial variance)] was plotted for each year (n = 31). The ordinary least-squares regression (OLS) was used to test the temporal TL by fitting the following equation (Eq. 1):

$\log_{10}(\text{temporal variance}) = \log_{10}(a_T) + b_T \times \log_{10}(\text{temporal mean})$.

Similarly, OLS was used for testing of the spatial TL:

$\log_{10}(\text{spatial variance}) = \log_{10}(a_S) + b_S \times \log_{10}(\text{spatial mean})$.

Pairwise cross-correlation coefficient between population growth rates (r_c, Pearson's correlation coefficient between population growth rates) was used as the index of population synchrony (Bjørnstad, Ims, & Lambin, 1999).

2.3 | Gompertz model

The second-order autoregressive model (the Gompertz model; Eq. 2) was used for describing population dynamics of the grey-sided vole. In this model, for each population j = 1,…, 85,

$x_{t,j}$ is the natural logarithm of the Bayesian estimate of an observed density ($N_{t,j}$) in periods of time t = 1962,…,1992; $\overline{x_j}$ is the temporal mean of $x_{t,j}$ in population j, and $x_{t,j} - \overline{x_j}$ is the centered time-series on the logarithmic scale of population j. The Gompertz model assumes that

$$x_{t,j} - \overline{x_j} = (1 + a_{1,j})(x_{t-1,j} - \overline{x_j}) + a_{2,j}(x_{t-2,j} - \overline{x_j}) + e_{t,j}\ , \qquad \text{(Eq. 2)}$$

where $a_{1,j}$ and $a_{2,j}$ are the coefficients of density dependence for a one-year lag and for a two-year lag for population j, respectively. The error term, $e_{t,j}$, represents the density-independent effects (environmental variability) modeled as random numbers from a normal distribution with mean = 0 and variance = SD_j^2. Fitting the Gompertz model (Eq. 2) to the centered time series, $x_{t,j} - \overline{x_j}$, yielded the Bayesian estimates of $a_{1,j}$, $a_{2,j}$, and SD_j (see Saitoh & Cohen 2018 for details).

2.4 | Simulations

The following five simulations were carried out and referred to here as "fundamental simulation", "parameter combination simulation", "environmental synchrony simulation", "density-dependent dispersal simulation", and "combined simulation of environmental synchrony and density-dependent dispersal". To distinguish simulated densities from a density estimate of an observed population $x_{t,j}$ in Eq. (2), the following equation of $y_{t,j}$ was used:

$$y_{t,j} = (1 + a_{1,j})(y_{t-1,j} - \overline{x_j}) + a_{2,j}(y_{t-2,j} - \overline{x_j}) + \overline{x_j} + e_{t,j}. \qquad \text{(Eq. 3)}$$

The initial two observed densities, $x_{1,j}$ and $x_{2,j}$ were used as the first two densities ($y_{1,j} = x_{1,j}$ and $y_{2,j} = x_{2,j}$) of each simulated population. The state variable in all the simulations was the centered log-transformed population density, $y_{t,j} - \overline{x_j}$.

2.4.1. Fundamental simulation

In the fundamental simulation, the population-specific estimates of $a_{1,j}$, $a_{2,j}$, and SD_j for the 85 observed populations were used, and a mean of the observed densities ($\overline{x_j}$) was used as the equilibrium density. The environmental variability, $e_{t,j}$, between any two different years (t) and among populations was assumed to be uncorrelated. For each population j, $e_{t,j}$ was drawn from independent random values that were normally distributed over mean = 0 and variance = SD_j^2, [$\mathcal{N}_{t,j}(0, SD_j^2)$] (see Saitoh & Cohen 2018 for details).

2.4.2. Parameter combination simulation

To examine the effects of the model parameters on the temporal (b_T) and spatial (b_S) slopes, the fundamental simulation was modified using comprehensive combinations of the model parameters. In the parameter combination simulation, a specific set of the parameters (a_1, a_2, and SD) was fed to each dataset of the 85 time series spanning 31 years ($y_{t,j}$): [1 + a_1] ranging from –1.95 to 1.95, in 0.05 increments, a_2 ranging from –0.975 to 0.975, in 0.05 increments, and SD ranging from 0.05 to 1.0, in 0.05increments. The combinations of [1 + a_1] and a_2 were restricted to the range in which the time series were sustainable, i.e., 1,600 combinations (see Saitoh and Cohen 2018 for details). As the simulations were carried out with 20 different SDs for each combination of [1 + a_1] and a_2, 32,000 datasets of 31 × 85 $y_{t,j}$ were generated. The rest of the simulation procedures was the same as those of the fundamental simulation. The generated values were then transformed back by exponentiating to the original scale of population density, and the temporal and spatial TLs were tested for each dataset.

2.4.3. Environmental synchrony simulation

To synchronize the time series, the 85 correlated density-independent error terms $e_{t,i}$, each of which consisted of 31 random numbers that were taken from a normally distributed values

with mean = 0 and variance = 1, were generated by using the "mvrnorm" function from the MASS package of R. The degree of the correlation between $e_{t,i}$ was given as a value (ρ) ranging from 0 to 1 in 0.001 increments, and ρ was used as an index of environmental synchrony. For each population j, the standard deviation of $e_{t,j}$ was adjusted to the observed one (SD_j). Estimates from the observed populations were used for other necessary values (equilibrium density, $[1 + a_1]$, and a_2) for the simulation.

The rest of the simulation procedures was the same as those of the fundamental simulation. One-thousand datasets (1,000 ρs) of the 85 time series were generated, and the temporal and spatial TLs were tested for each dataset.

2.4.4. Density-dependent dispersal simulation

Based on the concept of Perry (1988) and Ripa (2000), dispersal was assumed to occur when a population density exceeded an equilibrium density. The number of "surplus" individuals of a population, which were potential emigrants, was given by the subtraction of the equilibrium density from the simulated population density before the occurrence of the dispersal events $\left(y_{t,i} - \overline{x_i}\right)$. A part of the "surplus" individuals, $d\left(y_{t,i} - \overline{x_i}\right)$, may emigrate from their native population, but not all emigrants may survive until reaching the new colony, and, then, a population may accept some immigrants from emigrants of other populations. The population density after the occurrence of the density-dependent dispersal ($z_{t,i}$) can be given by the following equation:

$$z_{t,i} = y_{t,i} - d\left(y_{t,i} - \overline{x_i}\right) + \frac{s}{n}\sum_{i=1}^{n} d\left(y_{t,i} - \overline{x_i}\right), \qquad \text{(Eq. 4)}$$

when $\left(y_{t,i} - \overline{x_i}\right) < 0$, $\left(y_{t,i} - \overline{x_i}\right)$ was replaced with zero.

In Eq. 4, $y_{t,i}$ and $\overline{x_i}$ are defined in Eq. 3, d is the dispersal rate (a ratio of emigrants in "surplus" individuals), which was assumed to be a different value ranging from zero to one in 0.001 increments for each simulation, s is the success rate of dispersers colonization, which

was assumed to be 0.5 in this simulation, and each population was assumed to have accepted an equal number of immigrants, which was obtained by dividing the total number of successful dispersers by the number of populations (i.e., n = 85 in this case). As the number of dispersers should be zero or positive, when $\left(y_{t,i} - \bar{x_i}\right) < 0$, $\left(y_{t,i} - \bar{x_i}\right)$ was replaced with zero. This simulation did not include any effect of environmental synchrony.

The rest of the simulation procedures was the same as those of the fundamental simulation. One-thousand datasets (1,000 *d*s) of the 85 time series were generated, and the temporal and spatial TLs were tested for each dataset.

2. 4. 5. Combined simulation including environmental synchrony and density-dependent dispersal

Since the assumptions about environmental synchrony and density-dependent dispersal were not mutually exclusive, the effects of both the phenomena were included in the combined simulation, using comprehensive combinations of the environmental synchrony (ρ) and dispersal rate (d); ρ and d were independently increased from 0.001 to 1.0 in 0.001 increments. Estimates from the observed populations were used for other necessary values (equilibrium density, $[1 + a_1]$, a_2, and SD) for the simulation. One-million datasets (1,000 ρs × 1,000 *d*s) of the 85 time series were produced, and the temporal and spatial TLs were tested for each dataset.

2. 5. Factors that influence the slopes

Simulated time series have been defined by three model parameters (a_1, a_2, and SD) in the parameter combination simulation. The relationship between the variance and mean of the population densities and model parameters was analyzed by a multiple regression analysis, with the slope (b_T or b_S) as a response variable and with the model parameters as the

explanatory variables. All underlying regressions were computed using function "lm" in R version 3.6.0.

3 | RESULTS

3.1 | Empirical Taylor's laws

Both the temporal and spatial TLs were satisfied in the 85 empirical populations of the grey-sided vole (Fig. 1). The $\log_{10}$(temporal variance) of the population densities was approximated by a linear function of $\log_{10}$(temporal mean) of population densities (Fig. 1a): $\log_{10}$(temporal variance) = 0.063 (± SE 0.133) + 1.943 (± SE 0.143) × $\log_{10}$(temporal mean) (t = 13.576, $P < 2.0 \times 10^{-16}$, adjusted R^2 = 0.686), and the lower and upper limits of the 95% confidence interval (95%CI) of the estimate of the temporal slope (b_T) were 1.659 and 2.228, respectively. The $\log_{10}$(spatial variance) was also approximated by a linear function of $\log_{10}$(spatial mean) (Fig. 1b): $\log_{10}$(spatial variance) = 0.376 (± SE 0.125) + 1.579 (± SE 0.136) × $\log_{10}$(spatial mean) (t = 11.573, $P < 2.0 \times 10^{-12}$, adjusted R^2 = 0.816), and the lower and upper limits of 95%CI of the estimate of the spatial slope (b_S) were 1.300 and 1.858, respectively. The linearity of TLs was tested by quadratic regression analyses. These analyses did not reveal any statistically significant evidence of nonlinearity for the temporal or spatial relationship.

The index of population synchrony, pairwise cross-correlation coefficients of population growth rates (r_c) ranged from –0.390 to 0.935 (Fig. 1c). The mean of r_c values was 0.377 (SD = 0.199), and its lower and the upper quartile was 0.236 and 0.519, respectively. More than half of the pairs of populations (n = 1960, 54.9%) exhibited a significantly positive correlation ($r_c \geq 0.361$, $P < 0.05$). A significantly negative correlation was observed in two of 3,570 pairs, whose r_c values were –0.390 and –0.363, respectively.

3.2 | Simulated Taylor's law

3.2.1 Model parameters for slopes 1 < b < 2

To examine the effects of the model parameters on the temporal (b_T) or spatial (b_S) slopes, various combinations of the model parameters (n = 32,000) beyond the observed ones were input to the Gompertz model (Eq. 3) under the absence of correlations and density-dependent dispersal. All simulated datasets cleared the test of the temporal TL (Fig. 2a). A part (21.9%) of temporal slopes (b_T) (7,022/32,000) fell in the prevailing range ($1 < b_T < 2$). In other words, sustainable populations obeyed the temporal TL in the absence of environmental synchrony and density-dependent dispersal among populations, but only a limited proportion of those populations exhibited b_T that fell in the prevailing range.

Not all simulated datasets cleared the test of the spatial TL (Fig. 2b), but 84.7% of the simulated datasets (27,111/32,000) exhibited significantly positive spatial slopes (b_S). In simpler terms, most if not all sustainable populations obeyed the spatial TL under the conditions that excluded environmental synchrony and density-dependent dispersal. A quarter (25.6%) of b_S (8,199/32,000) fell in the prevailing range ($1 < b_S < 2$).

The percentage of datasets in which the two slopes simultaneously fell in the prevailing range ($1 < b_T < 2$ and $1 < b_S < 2$) was 8.2%.

The variance of b_S (0.841) was much higher than that of b_T (0.083, F-test, $F = 0.099$, $P < 2 \times 10^{-16}$, Fig. 2c). As a result, although a significant correlation was observed between b_S and b_T (Pearson's product-moment correlation coefficeint, $r_p = 0.623$, $P < 2 \times 10^{-16}$), one-on-one interaction between b_S and b_T was not clear (Fig. 2c). Even when datasets exhibiting significantly positive slopes were focused upon, the correlation between b_S and b_T could not be improved. These results imply that there may be some differences in the determinants and/or a mechanism of the TL formation between the temporal and spatial TLs.

A multiple regression analysis was performed on the temporal and spatial TLs, in which the slope b_T or b_S was considered as a response variable, while density dependence coefficients ([1 + a_1] and a_2), environmental variability (*SD*), and their pairwise products were used as explanatory variables (Table 1). These explanatory variables and their products contributed significantly to the explanation of variation of the slopes, and the full model exhibited a moderate goodness of fit (R^2 = 0.477 for the temporal TL and R^2 = 0.699 for the spatial TL). To summarize these results, the slopes became steeper with the increase of *SD* and with the decrease of a_1 and a_2. This pattern was found to be common between the temporal and spatial TLs. However, the absolute values of partial regression coefficients were found to be higher for the spatial TL than for the temporal TL, because the variance of b_S was much higher than that of b_T.

The model parameters that produced the prevailing range of slopes, $1 < b < 2$, were distributed over a limited range both for the temporal and spatial TLs (Fig. 3a, b). Density dependence coefficients ([1 + a_1] and a_2) exhibited a roughly similar pattern for the probabilities for $1 < b_T < 2$. A peak was found in the middle of the range for both coefficients (Figs. 3a1 and 3a2). The highest probability (0.409) was observed at [1 + a_1] = 0.15, while it was 0.380 when a_2 was 0.075. In contrast to this trend in the temporal TL, density dependence coefficients ([1 + a_1] and a_2) showed a different pattern for the probabilities for $1 < b_S < 2$ in the spatial TL. Although a clear peak of the probability (0.455) was observed for [1 + a_1] when it was –0.4 as in the temporal TL (Fig. 3b1), the probabilities for $1 < b_S < 2$ did not exhibit a clear pattern for a_2 (Fig. 3b2). The highest probability (0.336) was observed at a_2 = 0.175.

The simulated time series with a low *SD* exhibited higher probabilities for $1 < b_T < 2$ and for $1 < b_S < 2$. In the temporal TL, the highest probability for $1 < b_T < 2$ (0.523) was observed at *SD* = 0.05; the probabilities remained high values at low *SD* (0.05 to 0.20) and

plummeted thereafter (Fig. 3a3). The spatial slopes (b_S) responded to *SD* in a slightly different manner than the temporal slopes; the probabilities for $1 < b_S < 2$ fluctuated around 0.4 in $0.05 \leq SD \leq 0.4$ and declined thereafter (Fig. 3b3).

Differences in the effects of the model parameters between the temporal and spatial slopes are illustrated in Figure 4, where the probability for $1 < b_T < 2$ or $1 < b_S < 2$ is represented for each combination of $[1 + a_1]$ and a_2. Each cell of the combinations has 20 values of b_T and b_S, which were obtained from 20 different *SD* values. The number of $1 < b_T < 2$ or $1 < b_S < 2$ was counted for each cell, and the probabilities were calculated by dividing this counted number by the 20.

Cells with higher probabilities for $1 < b_T < 2$ were distributed on the center of the triangle and their distribution range was extended toward the upper-right cells. When plotting observed 85 populations on this panel based on their observed values of $[1 + a_1]$ and a_2, the observed populations fell in the distribution ranges of the higher probabilities (Fig. 4a). This suggests that the model parameters (a_1 and a_2) can predict the occurrence of the observed b_T.

Differing from the temporal TL, cells with higher probabilities for $1 < b_S < 2$ were widely scattered in an L-shaped pattern (Fig. 4b). The matching of the distribution ranges between the cells with higher probabilities and the observed populations was not well-defined. Many observed populations were plotted on the side of the lower probability areas, even though the observed b_S was 1.579. This discrepancy suggests that the explanatory power of the model parameters (a_1 and a_2) was limited for the observed b_S, and that the observed b_S may be influenced more by factors other than a_1 and a_2.

3.2.2. Fundamental effects of model parameters

The effects of the observed parameters of the Gompertz model were examined by the fundamental simulation without the consideration of the effect of environmental synchrony

and density-dependent dispersal using the population-specific estimates of $a_{1,j}$, $a_{2,j}$, and SD_j for the 85 observed populations. In the 10,000 simulated datasets, 30.2% of the simulated b_Ts were included in the 95%CI of the observed b_T (Fig. 5a1); whereas, all simulated b_Ss and indices of density synchrony (r_c) diverged from the observed ones (Figs. 5a2, a3). There were no simulated datasets in which b_T and b_S were simultaneously included in the 95%CI of the observed b_T and b_S.

The validity of the fundamental simulation was tested by comparing the temporal means and variances between observed and simulated values. Simulated means and variances were higher than observed ones, in general. In one example, although $\log_{10}$(observed means) showed a significant linear function of $\log_{10}$(simulated means), its slope was lower than 1; $\log_{10}$(observed mean) = 0.083 (± SE 0.067) + 0.847 (± SE 0.068) × $\log_{10}$(simulated mean) (t = 12.515, $P < 2.0 \times 10^{-16}$, adjusted R^2 = 0.650, Appendix Fig. Aa). A similar relationship was observed for variances; $\log_{10}$(observed variance) = 0.871 (± SE 0.186) + 0.444 (± SE 0.084) × $\log_{10}$(simulated variance) (t = 5.302, $P < 9.3 \times 10^{-7}$, adjusted R^2 = 0.244, Appendix Fig. Ab). The rate of the differences between observed and simulated values was higher in variances than in means. The simulated variances were 1.22 times as high as the observed variance on average, while the simulated means were 1.08 times as high as the observed means on average. The parameters of the Gompertz model (a_1 and a_2) did not show any effect on the differences between the observed and simulated values for both means and variances (Appendix Fig. Ae–h).

3.2.3. Environmental synchrony

Since a considerable proportion of population pairs (54.9%) exhibited significantly positive cross-correlations of population growth rates, the effects of environmental synchrony were added into the fundamental simulation. One-thousand datasets consisting of 85 time series

with different degrees of environmental synchrony (ρ, ranging from zero to one) were generated by the environmental synchrony simulation. Simulated temporal slopes (b_Ts) decreased with the increase of ρ and were described as a quadratic function of ρ (Fig. 6a1): b_T = 2.287 (± SE 0.013) + 0.094 (± SE 0.059) × ρ – 0.231 (± SE 0.057) × ρ^2. However, because of the low decrease rate, the simulated b_Ts did not decrease enough to be included in the 95%CI of the observed b_T.

Simulated spatial slopes (b_Ss) were described as a cubic function of ρ with a high predictability (Fig. 6a-2): b_S = 2.320 (± SE 0.012) – 2.687 (± SE 0.104) × ρ + 4.959 (± SE 0.242) × ρ^2 – 2.930 (± SE 0.159) × ρ^3. The simulated b_Ss greatly decreased with the increase of ρ between 0 and 0.3, and a considerable number of them were included in the 95%CI of the observed b_S, when ρ was greater than 0.4. However, the overlap between the simulated b_Ss and the 95%CI of the observed b_S was still limited.

The relationship between the index of population synchrony (r_c) and ρ was as clear as predicted from the theory. The degree of population synchrony was described as a linear function of ρ with a very high predictability (Fig. 6a3): r_c = 0.010 (± SE 0.003) + 0.866 (± SE 0.005) × ρ. Majority of r_cs fell in the interquartile range of the observed r_c, when ρ was between 0.3 and 0.5.

With ρ = 0.45, 10,000 datasets were generate based on the environmental synchrony simulation. While 98.0% of simulated r_cs were included in the interquartile range of the observed r_c, the proportion of the datasets in which b_T or b_S were included in the 95%CI of the observed slope was limited; 33.0% for b_Ts and 38.4% for b_Ss (Fig. 5b). The proportion of the datasets in which b_T and b_S were simultaneously included in the 95%CI of the observed slope was 14.7%.

3.2.4. Density-dependent dispersal

Since density-dependent dispersal could reduce the temporal and spatial variations of population densities (Abbott, 2011; Hastings, 1982), the effects of density-dependent dispersal were added into the fundamental simulation. One-thousand datasets consisting of 85 time series were generated by the density-dependent dispersal simulation. The temporal slopes were well described as a quadratic function of the dispersal rate (d = ratio of emigrants in "surplus" individuals, Fig. 6b1): $b_T = 2.330$ (± SE 0.011) – 0.193 (± SE 0.052) × d – 0.139 (± SE 0.051) × d^2. The simulated b_Ts decreased with the increase of d, and most of the simulated b_Ts were included in the 95%CI of the observed b_T, when d became higher than 0.6.

The spatial slopes were also described as a quadratic function of d (Fig. 6b2): b_S = 2.623 (± SE 0.013) – 0.020 (± SE 0.061) × d – 2.707 (± SE 0.058) × d^2. The simulated b_Ss greatly decreased with the increase of d. Most of the simulated b_Ss were included in the 95%CI of the observed b_S, when $0.5 < d < 0.7$.

Population synchrony (r_c) did not strongly respond to the change in d (Fig. 6b3). Although r_c was described as a quadratic function of d ($r_p = 0.021$ (± SE 0.001) + 0.033 (± SE 0.006) × d + 0.119 (± SE 0.006) × d^2, the regression coefficients were small. Although r_c increased with the increase of d, most r_cs did not reach the lower quartile value of the observed r_c.

With $d = 0.65$, 10,000 datasets were generated based on the density-dependent dispersal simulation. Most (80.4%) of the simulated b_Ts and 93.7% of the simulated b_Ss were included in the 95%CI of the observed b_T and b_S, respectively (Fig. 5c1, 5c2). Three-quarters (75.0%) of the datasets had realistic b_T and b_S values, both of which were included in the 95%CI of the observed value. However, all simulated r_cs were lower than the lower interquartile value of the observed r_c (Fig. 5c3).

3.2.5. Combined effects of synchrony and dispersal

The environmental synchrony simulation and the density-dependent dispersal simulations could not generate realistic datasets of which b_T, b_S, and r_c values could simultaneously satisfy the observed values. The proportion of the datasets that satisfied those conditions was 14.7% in the environmental synchrony simulation, while no datasets satisfied the same conditions in the density-dependent dispersal simulation. When just one of the effects (environmental synchrony or density-dependent dispersal) was considered, simulations based on the AR model were unable to generate a realistic set of time series for the observed populations. Hence, a combined simulation including both effects was carried out.

One-million datasets (1,000 ρs × 1,000 ds), each of which consisted of 85 time series, were organized into 10,000 cells (100 ρs × 100 ds in 0.01 increments for each parameter), each of which had 100 sets of three values (b_T, b_S, and r_c). The number of datasets which satisfied 1.659 (the lower limit of 95%CI) < b_T < 2.228 (the upper limit of 95%CI), 1.300 (the lower limit of 95%CI) < b_S < 1.858 (the upper limit of 95%CI), and 0.236 (the lower quartile) < r_c < 0.519 (the upper quartile) was counted for each cell, and the probabilities were calculated by dividing the counted number by 100. The highest probability (1.00) was observed in one cell with ρ = 0.241–0.250 and d = 0.521–0.530 (Appendix Fig. B).

With ρ = 0.245 and d = 0.525, 10,000 datasets were generated. Most (95.4%) of the simulated b_Ts and 98.3% of the simulated b_Ss were included in the 95%CI of the observed b_T and b_S, respectively (Fig. 5d). In addition, 98.8% of the simulated r_cs were included in the interquartile range of the observed r_c. On a whole, majority (92.7%) of the datasets satisfied all the three conditions simultaneously.

The observed density dependence coefficients (a_1 and a_2) were used for the above simulation analysis. To clarify the effects of density dependence coefficients on b_T and b_S, another combined simulation was carried out. In this simulation, 10,000 datasets were

generated, with $\rho = 0.245$ and $d = 0.525$, and using the hypothetical combinations of a_1 and a_2 that produced, with the lowest probability, the prevailing TL slopes. The coefficient a_1 and a_2 were randomly selected, not allowing replacement, from the combinations with the lowest probability producing $1 < b_T < 2$ and $1 < b_S < 2$. In the parameter combination simulation, those combinations were represented as black cells in Figures 4a and 4b; 228 cells illustrate the lowest probability (zero) for both b_T and b_S.

Although the majority of simulated r_cs (86.3%) were included in the interquartile range of the observed r_c, the proportion of simulated datasets of which b_T and b_S were included in the 95%CI of the observed values was lowered (Appendix Fig. C); it was 46.5% and 22.4% for b_T and b_S, respectively. The proportion of datasets simultaneously satisfying the three conditions was very small (4.4%).

4 | DISCUSSION

4.1 | Temporal and spatial Taylor's laws and population synchrony

The studied 85 populations of the grey-sided vole obeyed both the temporal and spatial TLs (Fig. 1ab). The temporal and spatial slope (95%CI) was estimated at 1.943 (1.65 – 2.228) and 1.579 (1.300 – 1.858), respectively. A considerable proportion of the observed populations (54.9%) exhibited a significantly positive cross-correlation of population growth rates (Fig. 1c). Taylor, Woiwod, and Perry (1980) provided datasets on the temporal and spatial TLs for populations of bird species. The mean temporal slope (range) was 1.13 (0.08 – 1.97, $n = 104$), while the mean spatial slope (range) was 1.71 (0.98 – 3.38, $n = 119$). Additionally, Linnerud et al. (2013) reported the temporal slopes for 30 populations of bird species; the mean slope (range) was 1.49 (0.69 – 2.24). Mellin, Huchery, and Caley (2010) reported spatial slopes for 18 fish species ranging between 1.16 and 1.84, while Kuo et al. (2016) reported that the mean

spatial slope (range) was 1.78 (1.41 – 2.11) in 29 fish species. The slopes for vertebrate populations appear to be lower than those for insect populations. The mean temporal slope (range) of aphids and moths are 1.86 (1.06 – 2.51, $n = 97$) and 1.50 (1.08 – 1.98, $n = 263$), respectively. The mean spatial slopes (range) for aphids and moths are 1.97 (1.29 – 2.95, $n = 97$) and 2.06 (0.08 – 3.32, $n = 263$), respectively (Taylor, Woiwod, & Perry 1980). Another report on 20 aphid species showed that temporal slopes ranged between 1.86 and 2.97, while spatial slopes between 1.89 and 2.67 (Zhao, Sheppard, & Reid, 2019). Both the observed slopes of the grey-sided vole fell in the prevailing range ($1 < b < 2$) and were consistent with the reported slopes for vertebrates.

4.2 | Similarity and dissimilarity between temporal and spatial TLs

Saitoh and Cohen (2018) demonstrated that some combinations of the model parameters of the Gompertz model (a_1, a_2, and SD) had the potential to explain the nature of the observed temporal TL using the same datasets analyzed in this study. However, in addition to the temporal TL, the spatial TL and population synchrony should be examined simultaneously to gain an overall understanding of the TLs governing empirical populations, because those three features may be related.

The parameter combination simulation showed that sustainable populations could obey both temporal and spatial TLs in the absence of population synchrony and density-dependent movements among populations (Fig. 2ab). However, the proportions of slopes that fell in the prevailing range ($1 < b < 2$) were limited to 21.9% for b_T and 25.6% for b_S, and the proportion of datasets in which both slopes simultaneously fell in the prevailing range was small (8.2%). The slopes became steeper with the increase of SD and with the decrease of a_1 and a_2 in both temporal and spatial TLs (Table 1). However, because of the higher variance of b_S, the absolute partial regression coefficients were much higher for the spatial TL than for

the temporal TL (Table 1, Fig. 2c). These results suggest that the power of the parameter combination simulation was limited to explaining the empirical range of TL slopes, and that the degree of factors influencing the TL formation may differ between the temporal and spatial TLs.

Differences between the temporal and spatial TLs in terms of the effects of model parameters on the slopes are illustrated in Figure 4, where the probability for $1 < b_T < 2$ or $1 < b_S < 2$ is represented for each combination of $[1 + a_1]$ and a_2. The majority of the observed populations coincided with the cells with higher probabilities for $1 < b_T < 2$, while the distribution range of the cells with higher probabilities for $1 < b_S < 2$ did not closely match that of the observed populations. Some observed populations were plotted on the lower probability cells for $1 < b_S < 2$, even though the observed b_S was 1.579. This discrepancy suggests that the observed b_S may be influenced more by factors other than a_1 and a_2.

4.3 | Environmental synchrony and density-dependent dispersal

Population synchrony should be examined on priority because a considerable proportion of the observed populations exhibited a significantly positive cross-correlation of population growth rates, and because the negative effects of the density correlation on the spatial TL slopes were reported in populations of aphid and plankton species (Reuman et al., 2017). Population synchrony represents the spatial synchrony of the abundance and may arise from three primary mechanisms (Liebhold, Koenig, & Bjørnstad, 2004): (1) dispersal among populations, (2) synchronous exogenous density-independent factor known as the Moran effect (Moran 1953), and (3) trophic interaction with other species. In this study, the effects of environmental synchrony and density-dependent dispersal were explicitly examined through the environmental synchrony and the density-dependent dispersal simulations, respectively. Although the effects of the trophic interaction were not directly specified or

explored in this study, the effects involved in the density-dependent dispersal simulation could arise from density-dependent predation (see below).

In majority of the cases, the environmental synchrony and density-dependent dispersal simulations could not generate datasets for which b_T, b_S, and r_c simultaneously satisfied the observed values by its assumed mechanism alone (Fig. 5bc). The proportion of datasets that satisfied those conditions in the environmental synchrony simulation was 14.7%, when the degree of environmental synchrony (ρ) was set to the most possible value (0.45), while no dispersal rate (d) was found to satisfy those conditions in the density-dependent dispersal simulation.

When only one of the effects (environmental synchrony or density-dependent dispersal) was considered, simulations based on the Gompertz model could not generate a realistic set of time series for the observed populations. Both the effects were required to generate datasets that satisfied those conditions. In the 10,000 datasets generated by the combined simulation with $\rho = 0.245$ and $d = 0.525$, majority of the datasets (92.7%) satisfied the three conditions. The Gompertz model considered in this study consisted of two types of density effects (a_1 and a_2) and the density-independent effect (e_t, Eq. 2). The synchrony of population density was simulated by synchronizing e_t within the Gompertz model of this study. The effects of a_1 and a_2 are derived from the densities in the one-year (x_{t-1}) and two-year lags (x_{t-2}), respectively. Although the effects in the current year were considered as the density-independent term (e_t), the density effect from the current year (x_t) was not considered. The effects of density-dependent dispersal are derived from x_t and were needed to generate datasets that satisfied the required conditions.

In the model of this study, dispersal was assumed to occur when a population density in the current year exceeded the equilibrium population density, and 52.5% of "surplus" individuals ($d = 0.525$) emigrated from the native population in the combined simulation.

Although the loss due to dispersal was partly compensated by the immigrants, the main effect of dispersal in this simulation was the density-dependent loss. Therefore, the combined simulation consisted of three types of density effects from three different time phases (the current year, the one-year lag, and the two-year lag). Among those effects, the two slopes (b_T and b_S) were more sensitive to density-dependent dispersal (Fig. 6), and, thus, the density effects in the current year (density-dependent dispersal) may be the key to the determination of b_T and b_S.

In the density-dependent dispersal simulation, a part of "surplus" individuals emigrated from their home population, half of the emigrants were assumed to expire before reaching a new colony, and each population accepted an equal number of immigrants. A theoretical study shows that positive density dependent-dispersal is favored in temporally variable environments with high dispersal cost, whereas negative density-dependent dispersal benefits in stable environments with low dispersal cost (Rodrigues & Johnstone, 2014). Since the studied dataset includes highly fluctuating populations (Saitoh et al. 1997, 1998), the positive density-dependent dispersal (emigration) assumed in this study could be justified theoretically. However, many empirical researches suggest negatively density-dependent dispersal, although some convincing evidence of positive density-dependent dispersal does exist (Le Galliard et al. 2012). For the grey-sided vole, Ehrich, Yoccoz, and Ims (2009) showed that populations with multi-annual density fluctuations exhibited high genetic diversity even on the low density phase and suggested negatively density-dependent immigration, whereas the best model explaining the variation of genetic diversity suggested the positive effect of population growth rate and density in the common vole (*Microtus arvalis*, Gauffre et al. 2014). These contradictory observations may be attributed to the elusive nature of dispersal that may change conditionally (Matthysen, 2005). De Bona et al. (2019) showed in wild guppies that local density-dependent dispersal varied between positive

and negative, responding to landscape density. Further empirical studies on the effects of density on dispersal are encouraged to detail the effects of dispersal on TLs.

Positive density-dependent dispersal could have the effects to reduce the temporal and spatial variations of population densities (Abbott 2011; Hastings, 1982) and could potentially reduce the slopes b_T and b_S. In fact, the density-dependent dispersal simulation of this study showed the significantly negative effect of dispersal rate on both the slopes (Fig. 6b1, 6b2). In contrast to this finding, Engen, Lande, and Saether (2008) theoretically showed that increasing dispersal made the transition from slope 1 to 2. They examined the effects of sampling scale on TL considering individual dispersal and attributed their result to increasing scale in the spatial covariance function for population density with increasing dispersal. Although the 85 populations analyzed in this study had the spatial structure (see the map in Saitoh et al. 1997), the dispersal of individual voles among specific populations is unknown. Therefore, this study analyzed the overall effects of dispersal on TLs. The present findings should be carefully compared to those of Engen et al. (2008).

In the density-dependent dispersal simulation, a key process affecting the slopes was the partial loss of "surplus" individuals. Although the density-dependent dispersal simulation and the combined simulation attribute the density-dependent loss to dispersal, another mechanism can also explain the partial loss of "surplus" individuals. Mobile predators that travel long distance may assemble in high-density populations and take some parts of "surplus" individuals (e.g., Ims & Andressen, 2000). This is listed as a primary mechanism of the spatial synchrony of the abundance (trophic interaction) (Liebhold, Koenig, & Bjørnstad, 2004).

Although dispersal has been credited with inducing synchrony of population density (Abbott 2011), such an effect was miniscule in the present conditions of the simulations (Fig. 6b3). Local density-dependent dispersal may result in lower synchrony than comparable

amounts of density-independent dispersal (Abbott, 2011), which is the case of this study. Empirically, the dispersal ability of the grey-sided vole is too small (most natal dispersals of individuals are recorded within several hundred meters; Ishibashi & Saitoh 2008) to directly link with the studied populations, which were separated by an average distance of 8.4 km. The source of synchrony in the studied populations may be a large-scale climate variation or effects of nomadic predators (Bjørnstad, Stenseth, & Saitoh, 1999). In general, dispersal is not an essential driver of synchrony, because the population synchrony is often observed among isolated habitats between which dispersal is strictly limited (e.g., Grenfell et al., 1998; Rusak, Yan, & Somers, 2008). In addition, the Moran effect dominates over the effects of dispersal in spatial synchrony in forest insect populations (Peltonen et al., 2002), and Haynes et al. (2013) and Allstadt et al. (2015) claim the importance of weather effects as a driver of population synchrony.

The degree of density-dependent loss may vary among populations inhabiting various habitats. Effects of density-dependent loss may not be strong for populations in varying habitats because of vast environmental effects. For instance, insect populations, which inhabit agricultural ecosystems, may suffer high environmental variability, as they experience repeated extinction and colonization events between cultivation and non-cultivation seasons. Therefore, they may exhibit steeper slopes. In contrast, populations in stable habitats, such as vertebrate populations, may show greater density-dependent loss, because biological regulation likely works in those habitats, and, thus, their slopes may become more gradual. In fact, Park, Tayler, and Grewal (2013) observed steeper TL slopes in nematode in *r*-strategist populations. The temporal and spatial TL slopes may reflect life history variation (Linnerud et al., 2013; Park, Tayler, & Grewal, 2013; Samaniego, Sérandour, & Milne, 2012). Therefore, studies on the relationship of TL slopes to life history must be conducted to

elucidate the process of determining b_T and b_S, and they may also contribute to providing deeper insights into the biological interpretation of the slopes.

4.4 | Temporal and spatial variance

The variance of the spatial slopes (b_S) was greater than that of the temporal slopes (b_T). This difference was observed in the parameter combination simulation (Fig. 2), the environmental synchrony simulation (Fig. 6a), and the density-dependent dispersal simulation (Fig. 6b). These differences indicate that population densities are more strongly bound for the temporal TL than for the spatial TL within the conditions of this study.

The temporal variance of population densities is determined by the interplay between density dependence and environmental variability (Saitoh and Cohen 2018). The temporal slopes increased with the increase of environmental variability and decreased with the increase of density dependence coefficients (Table 1).

The spatial variation of population densities primarily depends on the variation of mean densities of the observed populations. The spatial variation was also affected by the temporal variation of population densities because a population temporally fluctuates around the equilibrium density (the mean observed density in this study). The primal spatial variation may be enhanced in highly fluctuating populations by the temporal divergence of population densities from the equilibrium density, but not so in less fluctuating populations. Therefore, the variance of b_S may be greater than the variance of b_T. This pattern was demonstrated by the fundamental simulation (Fig. 5a1,5a2).

The generality of this discussion can be tested by comparing temporal slopes with spatial slopes after taking the variation of life history into consideration. In empirical studies, variances are higher for the spatial slopes (b_S) than for the temporal slopes (b_T); b_S: 0.092 vs b_T: 0.073 for aphids; b_S: 0.142 vs b_T: 0.023 for moths; b_S: 0.129 vs b_T: 0.080 for Birds

(Taylor, Woiwod, & Perry,1980), while Zhao, Sheppard, and Reid (2019) reported inconsistent patterns in the variances of TL slopes among aphid species, plankton groups, and chlorophyll concentrations. Further comparative studies on temporal and spatial slopes in populations with various life histories may contribute to identifying the origin of the variation of population densities and will provide a deeper insight into the formation of TLs.

ACKNOWLEDGMENTS

I thank Joel E. Cohen for taking me to researches on Taylor's law and Andrew M. Liebhold for his helpful comments on an early draft of this manuscript. I also thank Eric Post, Nigel G. Yoccoz, and an anonymous reviewer for their comments. A Grant-in-Aid from the Japan Society for the Promotion of Science (no. 17K07552) partly supported this study. I have no conflicts of interest to declare.

REFERENCES

Abbott, K. C. (2011) A dispersal-induced paradox: synchrony and stability in stochastic metapopulations. *Ecology Letters*, 14, 1158–1169.

Allstadt, A. J., Liebhold, A. M., Johnson, D. M., Davis R. E., Haynes, K. J. (2015) Temporal variation in the synchrony of weather and its consequences for spatiotemporal population dynamics. *Ecology*, 96, 2935–2946.

Bjørnstad, O. N., Ims, R. A., Lambin, X. (1999) Spatial population dynamics: analyzing patterns and processes of population synchrony. *Trends in Ecology and Evolution*, 14, 427–432.

Bjørnstad, O. N., Stenseth, N. C., Saitoh, T. (1999) Synchrony and scaling in dynamics of voles and mice in northern Japan. *Ecology*, 80, 622–637.

Cohen, J. E. and Saitoh, T. (2016) Population dynamics, synchrony, and environmental quality of Hokkaido voles lead to temporal and spatial Taylor's laws. *Ecology*, 97, 3402–3413.

De Bona, S., Bruneaux, M., Lee, A. E. G., Reznick, D. N., Bentozen, P., Lopez-Sepulcre, A. (2019) Spatio-temporal dynamics of density-dependent dispersal during a population colonisation. *Ecology Letters*, 22, 634–644. doi: 10.1111/ele.13205

Downing, J. A. (1986) Spatial heterogeneity: evolved behaviour or mathematical artefact? *Nature*, 323, 255–257.

Ehrich, D., Yoccoz, N.G., Ims, R.A. (2009) Multi-annual density fluctuations and habitat size enhance genetic variability in two northern voles. *Oikos*, 118, 1441–1452.

Eisler, Z., Bartos, I., Kertész, J. (2008) Fluctuation scaling in complex systems: Taylor's law and beyond. *Advances in Physics*, 57, 89–142.

Engen, S., Lande, R., Saether, B-E. (2008) A general model for analyzing Taylor's spatial scaling laws. *Ecology*, 89, 2612–2622.

Gauffre, B., Berthier, K., Inchausti, P., Chaval, Y., Bretangnolle, V., Cosson, J.-F. (2014) Short-term variations in gene flow related to cyclic density fluctuations in the common vole. Molecular Ecology, 23, 3214–3225.

Grenfell, B. T., Wilson, K., Finkenstadt, B. F., Coulson, T. N., Murray, S., Albonk, S. D., Pemberton, J. M., Clutton-Brock, T. H., Crawley, M. J. (1998) Noise and determinism in synchronized sheep dynamics. *Nature*, 394, 674–677.

Hastings, A. (1982) Dynamics of a single species in a spatially varying environment: The stabilizing role of high dispersal rates. *Journal of Mathematical Biology*, 16, 49–55.

Haynes, K. J., Bjørnstad, O. N., Allstadt, A. J., Liebhold, A. M. (2013) Geographical variation in the spatial synchrony of a forest-defoliating insect: isolation of environmental and spatial drivers. *Proceedings of the Royal Society B*, 280, 20122373

Ims, R. A. and Andreassen, H. (2000) Spatial synchronization of vole population dynamics by predatory birds. *Nature*, 408, 194–196.

Ishibashi, Y. and Saitoh, T. (2008) Role of male-biased dispersal in inbreeding avoidance in the grey-sided vole (*Myodes rufocanus*). *Molecular Ecology*, 17, 4887–4896.

Kaneko, Y., Nakata, K., Saitoh, T., Stenseth, N. C., Bjørnstad, O. N. (1998) The biology of the vole *Clethrionomys rufocanu*s: a review. *Researches on Population Ecology*, 40, 21-37.

Kendal, W. S. (2004) Taylor's ecological power law as a consequence of scale invariant exponential dispersion models. *Ecological Complexity*, 1, 193–209.

Kuo, T. C., Mandal, S., Yamauchi, A., Hsieh, C. H. (2016) Life history traits and exploitation affect the spatial mean-variance relationship in fish abundance. *Ecology*, 97, 1251–1259.

Le Galliard, J.-F., Remy, A., Ims, R. A., Lambin, X. (2012) Patterns and processes of dispersal behaviour in arvicoline rodents. *Molecular Ecology*, 21, 505–523.

Liebhold, A., Koenig W. D., Bjørnstad, O. N. (2004) Spatial synchrony in population dynamics. *Annual Review of Ecology, Evolution, and Systematics*, 35, 467–490.

Linnerud, M., Saether, B-E, Grøtan, V., Engen, S., Noble, D. G., Freckleton, R. P. (2013) Interspecific differences in stochastic population dynamics explains variation in Taylor's temporal power law. *Oikos*, 122, 1207–1216.

Matthysen E (2005) Density-dependent dispersal in birds and mammals. Ecography 28:403–416. doi: 10.1111/j.0906-7590.2005.04073.x

Mellin, C., Huchery, C., Caley, M. J. (2010) Reef size and isolation determine the temporal stability of coral reef fish populations. *Ecology*, 91, 3138–3145.

Moran, P. (1953) The statistical analysis of the Canadian lynx cycle. II. Synchronization and meteorology. *Australian Journal of Zoology*, 1, 291–298.

Park, S-J, Tayler, R. A. J., Grewal, P. S. (2013) Spatial organization of soil nematode communities in urban landscapes: Taylor's power law reveals life strategy characteristics. *Applied Soil Ecology*, 64, 214–222.

Peltonen, M. Liebhold, A. M., Bjørnstad, O. N., Williams, D. W. (2002) Spatial synchrony in forest insect outbreaks: Roles of regional stochasticity and dispersal. *Ecology*, 83, 3120–3129.

Perry, J.N. (1988) Some models for spatial variability of animal species. *Oikos*, 51, 124-130.

Reuman, D. C., Zhao, L., Sheppard, L. W., Reid, P. C., Cohen, J. E. (2017) Synchrony affects Taylor's law in theory and data. *Proceedings of National Academy of Sciences of the United States of America*, 183, 6788–6793.

Ripa, J. (2000) Analysing the Moran effect and dispersal: their significance and interaction in synchronous population dynamics. *Oikos*, 89, 175–187.

Rodrigues, A. M. M., and Johnstone, R. A. (2014) Evolution of positive and negative density-dependent dispersal. *Proceedings of the Royal Society B*, 281, 20141226–8. doi: 10.1098/rspb.2014.1226

Rusak, J. A. Yan, N. D., Somers, K. M. (2008) Regional climatic drivers of synchronous zooplankton dynamics in north-temperate lakes. *Canadian Journal of Fisheries and Aquatic Sciences*, 65, 878–889.

Saitoh, T., Stenseth, N. C., Bjørnstad, O. N. (1997) Density dependence in fluctuating grey-sided vole populations. *Journal of Animal Ecology*, 66, 14–24.

Saitoh, T., Stenseth, N. C., Bjørnstad, O. N. (1998) Population dynamics of the vole *Clethrionomys rufocanu*s in Hokkaido, Japan. *Researches on Population Ecology*, 40, 61–76.

Saitoh, T. and Cohen, J. E. (2018) Environmental variability and density dependence in the temporal Taylor's law. *Ecological Modelling*, 387, 134–143.

Samaniego, H., Sérandour, G., Milne, B. T. (2012) Analyzing Taylor's scaling law: qualitative differences of social and territorial behavior on colonization/extinction dynamics. *Population Ecology*, 54, 213–223.

Spiegelhalter, D. J., Thoma, A., Best, N. G., Lunn, D. (2003) WinBUGS user manual (version 1.4). MRC Biostatistics Unit, Institute of Public Health, Cambridge

Stenseth, N. C., Viljugrein, H., Saitoh, T., Hansen, T. F., Kittilsen, M. O., Bølviken, E., Glöckner, F. (2003) Seasonality, density dependence, and population cycles in Hokkaido voles. *Proceedings of National Academy of Sciences of the United States of America*, 100, 11478–11483.

Taylor, L. R. (1961) Aggregation, variance and the mean. *Nature*, 189, 732–735.

Taylor, L. R. (1986) Synoptic dynamics, migration and the Rothamsted insect survey: Presidential Address to the British Ecological Society, December 1984. *Journal of Animal Ecology*, 55, 1–38.

Taylor, L. R., Woiwod, I. P., Perry, J. N. (1980) Variance and the large-scale spatial stability of aphids, moths and birds. *Journal of Animal Ecology*, 49, 831–854.

Taylor, L. R. and Taylor, R. (1977) Aggregation, migration and population mechanics. *Nature*, 265, 415–421.

Taylor, L. R. and Woiwod, I. P. (1982) Comparative synoptic dynamics. I. Relationships between inter- and intra-specific spatial and temporal variance/mean population parameters. *Journal of Animal Ecology*, 51, 879–906.

Tippett, M. K. and Cohen, J. E. (2016) Tornado outbreak variability follows Taylor's power law of fluctuation scaling and increases dramatically with severity. *Nature Communications,* 7, 10668.

Zhao, L., Sheppard, L. W., Reid, P. C. (2019) Proximate determinants of Taylor's law slopes. *Journal of Animal Ecology*, 88, 484–494.

TABLE 1 Summary of the results of multiple regression analyses of the effects of environmental variability (*SD*) and density dependence ([1 + a_1] and a_2) on the temporal slope b_T (A) and the spatial slope b_S (B) of Taylor's law using datasets generated by the parameter combination simulation (see the main text). A response variable was the slope (b_T or b_S), and explanatory variables were [1 + a_1], a_2, and *SD*. The primary model consisted of the three explanatory variables and all their multiplicative products. The primary model was selected as the best model by stepAIC. PRC = partial regression coefficient, SE = standard error of estimate.

The primary model: b_T (or b_S) ~ [1 + a_1] + a_2 + *SD* + [1 + a_1]:a_2 + a_1:*SD* + a_2:*SD* + [1 + a_1]:a_2:*SD*

	(A) Temporal TL		(B) Spatial TL	
	PRC	*SE*	PRC	*SE*
Intercept	1.910	0.003	0.553	0.007
1 + a_1	–0.502	0.006	–1.545	0.015
a_2	–0.516	0.005	–1.226	0.012
SD	0.433	0.005	2.502	0.012
[1 + a_1]:a_2*	–0.473	0.009	–1.132	0.022
[1 + a_1]:*SD**	0.525	0.010	1.617	0.025
a_2:*SD**	0.475	0.009	1.388	0.021
[1 + a_1]:a_2:*SD**	0.442	0.015	1.490	0.037

(A) *F*-statistic: 4162 on 7 and 31992 DF, *P*-value: $< 2 \times 10^{-16}$, adjusted R^2: 0.477

(B) *F*-statistic: 1.06×10^4 on 7 and 31992 DF, *P*-value: $< 2 \times 10^{-16}$, adjusted R^2: 0.699

* ":" represents a product of variables.

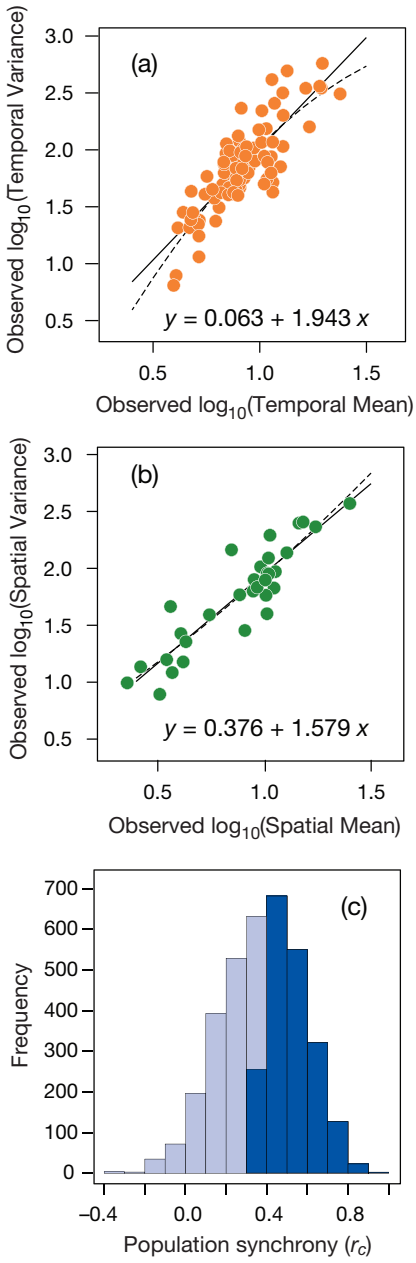

Figure 1 Temporal and spatial Taylor's laws of observed populations, and frequency distribution of pairwise cross-correlation coefficients (r_c) between population growth rates. (a) A scatter plot of $\log_{10}$(temporal variance) as a function of $\log_{10}$(temporal mean) of observed population densities estimated by a Bayesian method (see the main text) from 31 years (t = 1962, …, 1992) for 85 grey-sided vole populations (n = 85). (b) A scatter-plot of $\log_{10}$(spatial variance) as a function of $\log_{10}$(spatial mean) of observed population densities from 85 populations for 31 years (n = 31). The solid lines and the equations are obtained from the ordinary least-squares linear regression (OLS) of $\log_{10}$(variance) against $\log_{10}$(mean). The curved dotted line comes from the least-squares quadratic regression. (c) Frequency distribution of pairwise cross-correlation coefficients (r_c) between population growth rates of observed populations as an index of population synchrony (n = 3,570). The dark shaded areas indicate the significantly positive cross-correlation coefficients ($r_c \geq 0.361$, $P < 0.05$).

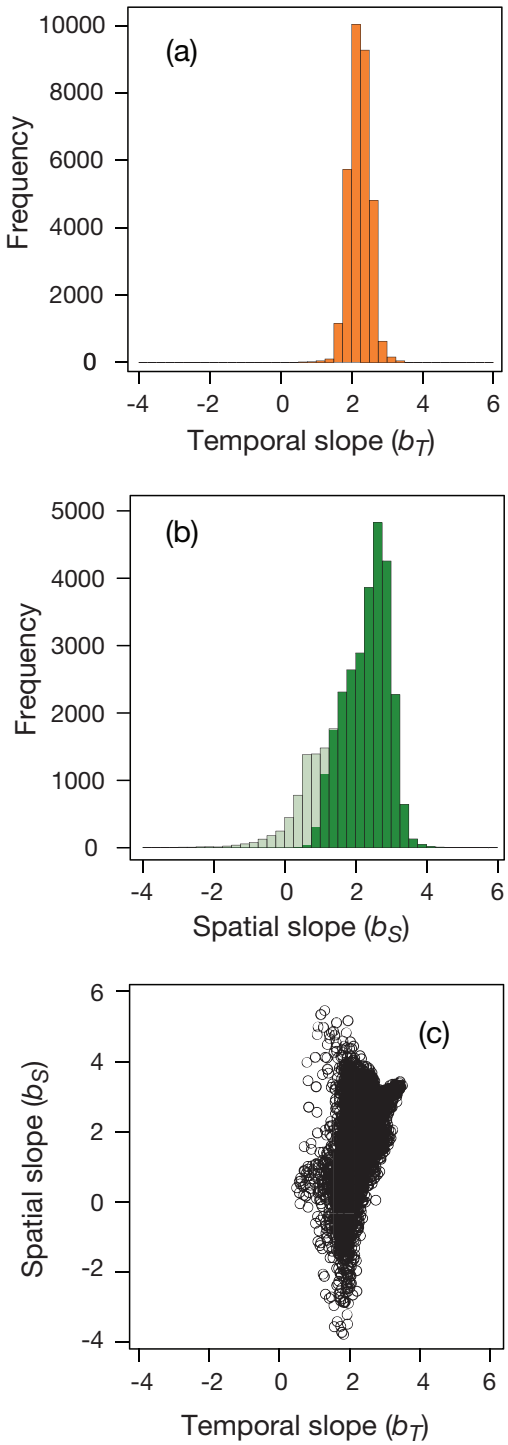

Figure 2 Frequency distributions of simulated TL slopes in the parameter combination simulation (see the main text for details). Thirty-two-thousand datasets, each of which consisted of 85 populations over 31 years, were produced. (a) Frequency distribution of the simulated slope b_T of the temporal TL (range: 0.493 to 3.508). The dark shaded areas indicate the frequency of data sets in which a simulated b_T was significantly higher than zero. (b) Frequency distribution of the simulated slope b_S of the spatial TL (range: –3.790 to 5.441). The dark shaded areas indicate the frequency of data sets in which a simulated b_S was significantly higher than zero. (c) A scatter-plot of the spatial slopes (b_S) for the temporal slopes (b_T).

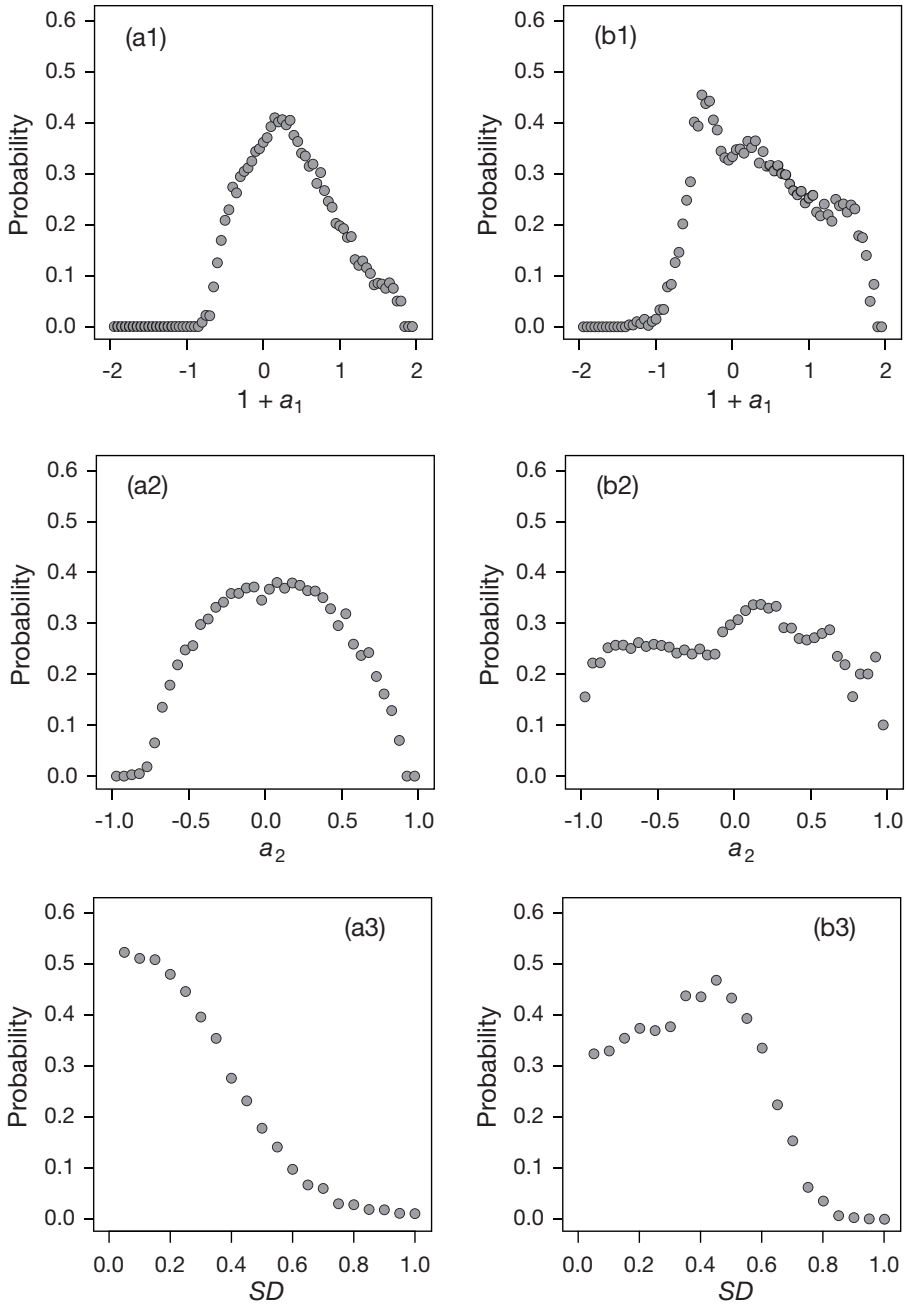

Figure 3 Probability that each of the three model parameters (a_1, a_2, and SD) of the Gompertz model produced TL slopes with $1 < b < 2$. Thirty-two-thousand data sets, each of which consisted of 85 populations over 31 years, were produced using various combinations of the model parameters on the parameter combination simulation (see the main text for details). (a1) The probability for $1 < b_T < 2$ is represented for 79 values of the density dependence coefficient with one-year lag ($1 + a_1$). (a2) The probability for $1 < b_T < 2$ is represented for 40 values of the density dependence coefficient with two-year lag (a_2). (a3) The probability for $1 < b_T < 2$ is represented for 20 values of the environmental variability parameter (SD). (b1) The probability for $1 < b_S < 2$ is represented for 79 values of the density dependence coefficient with one-year lag ($1 + a_1$). (b2) The probability for $1 < b_S < 2$ is represented for 40 values of the density dependence coefficient with two-year lag (a_2). (b3) The probability for $1 < b_S < 2$ is represented for 20 values of the environmental variability parameter (SD).

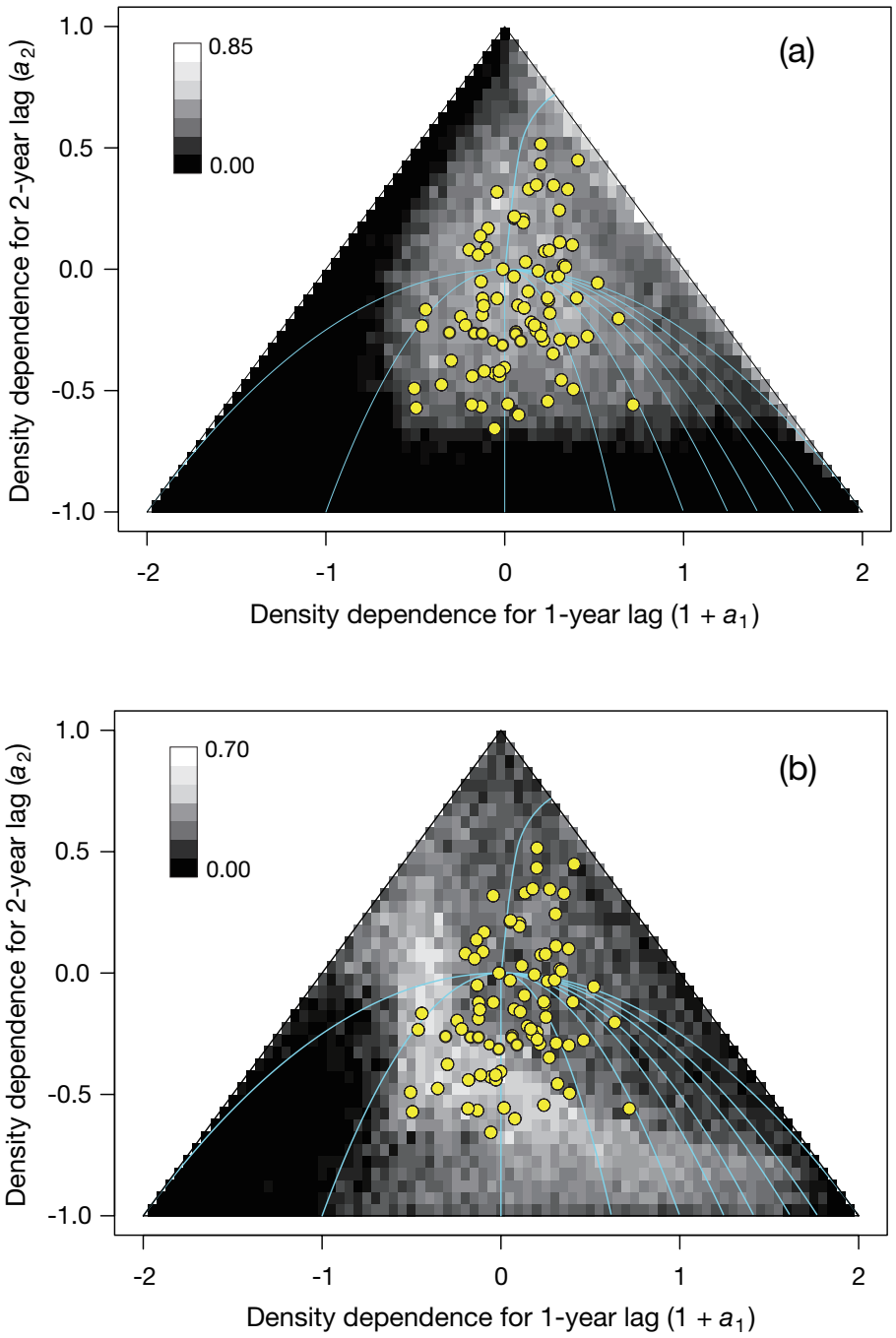

Figure 4 Relationship between TL slopes and density dependent coefficients ([1 + a_1] and a_2) in the parameter combination simulation. The shading of each cell indicates the probability for $1 < b < 2$ for each combination of density dependent coefficients ([1 + a_1] and a_2) in the range of *SD* between 0.05 and 1. The lighter shaded region indicates higher probability. Observed populations of the Hokkaido vole are illustrated by yellow circles (n = 85). (a) The probability of a temporal slope for $1 < b_T < 2$. The highest probability was 0.85. (b) The probability of a spatial slope for $1 < b_S < 2$. The highest probability was 0.70.

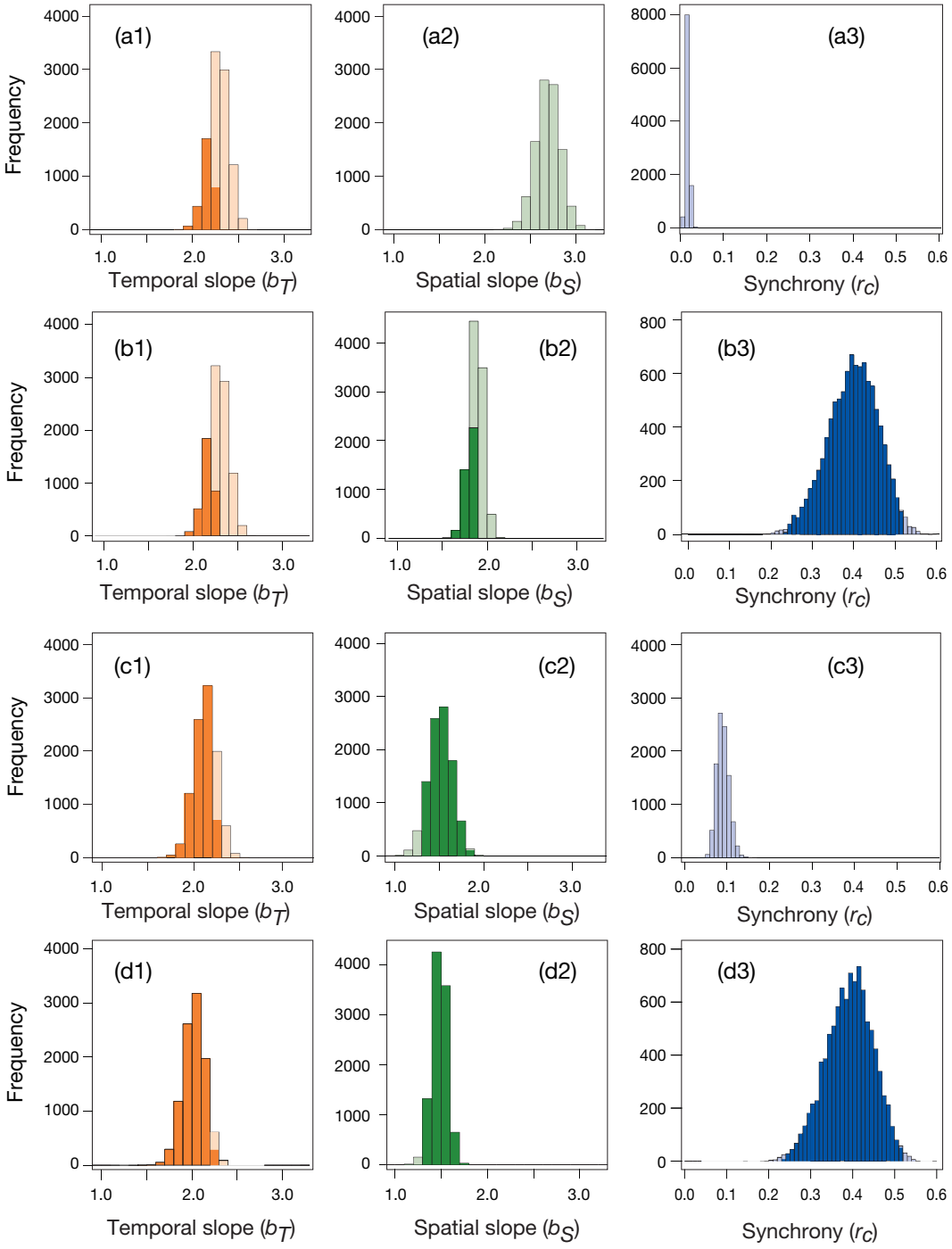

Figure 5 Frequency distributions of simulated TL slopes and the degree of population synchrony. Ten-thousand datasets, each of which consisted of 85 populations over 31 years, were produced in the following four simulation analyses: (a1–a3) the fundamental simulation, (b1–b3) the environmental-synchrony simulation, (c1–c3) the density-dependent dispersal simulation, and (d1–d3) the combined simulation (see the main text for simulation procedures). The dark shaded areas indicate the frequency of datasets in which the simulated temporal (b_T) or spatial (b_S) slopes were included in the 95%CI of the observed slope. For population synchrony which is represented as a pairwise cross-correlation coefficient (r_c) between population growth rates, the frequencies of data sets with a simulated r_c in the interquartile range of the observed value are illustrated in the dark shaded areas.

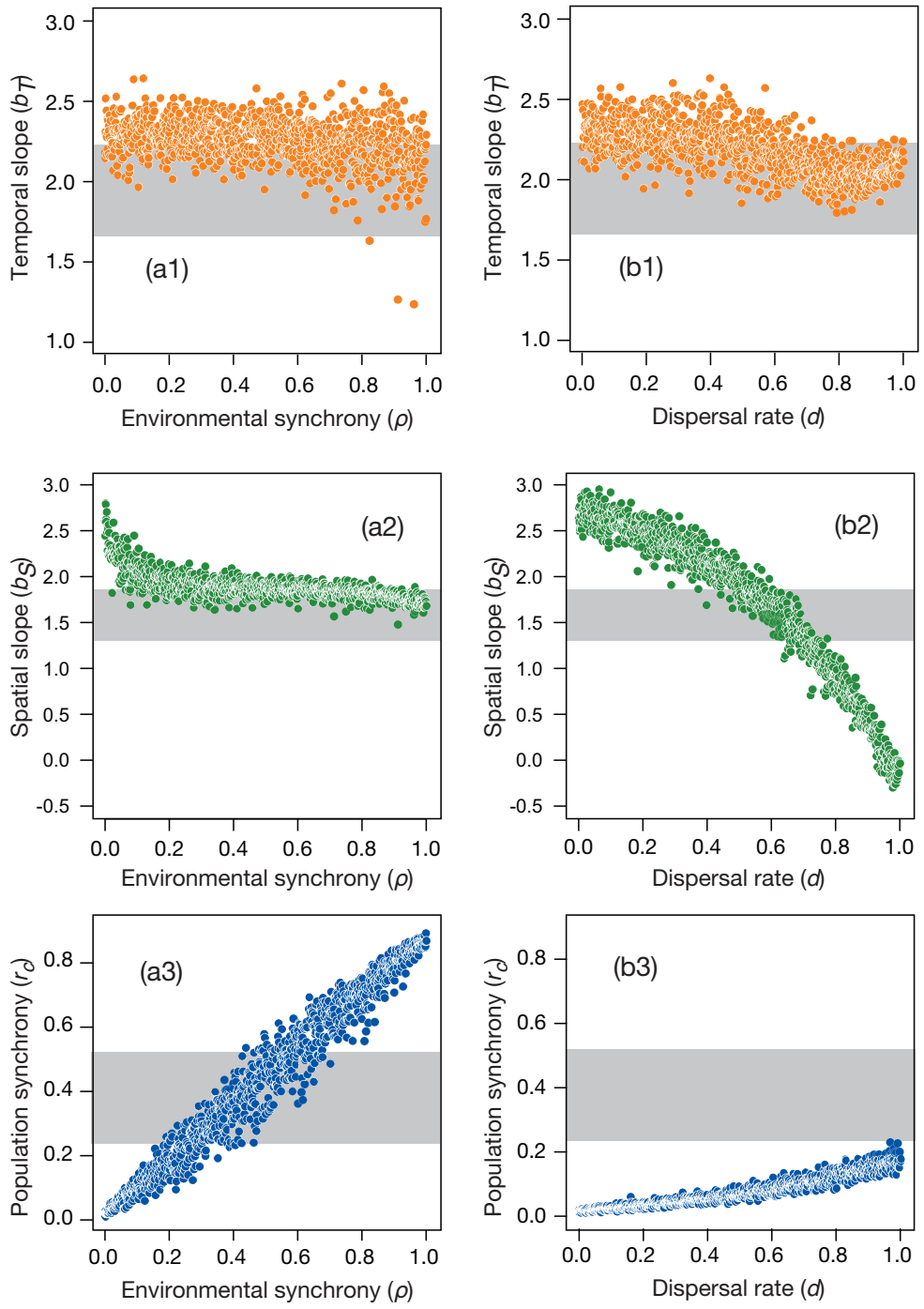

Figure 6 Scatter plots of temporal (b_T) and spatial (b_S) slopes for an index of environmental synchrony (ρ) and density-dependent dispersal rate (d), and the degree of population synchrony (r_c) for ρ or d. (a1) A scatter plot of the temporal slope (b_T) for environmental synchrony. The gray zone indicates the range of 95%CI for the observed b_T. (a2) A scatter plot of the spatial slope (b_S) for environmental synchrony. The gray zone indicates the range of 95%CI for the observed b_S. (a3) A scatter plot of population synchrony for environmental synchrony. The gray zone indicates the interquartile range of the observed r_cs. (b1) A scatter plot of the temporal slope (b_T) for dispersal rate. The gray zone indicates the range of 95%CI for the observed b_T. (b2) A scatter plot of the spatial slope (b_S) for dispersal rate. A gray zone indicates the range of 95%CI for the observed b_S. (b3) A scatter plot of population synchrony for dispersal rate. The gray zone indicates the interquartile range of the observed r_cs.